

The Effects of Residual Copper on Laser-Welded Low-Carbon Sheet Steels

The influences of increasing residual copper content on laser weldability and mechanical properties were evaluated

BY H. GEERLINGS, G. THOMAS, A. CLARKE, K. CLARKE, AND J. KLEMM-TOOLE

Abstract

With the increasing utilization of scrap in steelmaking, undesirable elements such as copper accumulate in the scrap stream, leading to inevitable enrichment in steel products. Many steel grades have limits on copper content due to thermomechanical processing problems, most notably hot-shortness. Still, the limit at which copper begins to negatively affect subsequent fabrication processes is largely unknown. This work investigated the influence of residual copper content, up to 0.83 wt-%, on the laser weldability and mechanical behavior of low-carbon sheet steels. The alloys were intercritically annealed prior to autogenous laser welding, cross-weld tensile testing, and weldability testing using the Sigmajig test. It was found that the increased amount of martensite/austenite constituent imparted by copper's stabilization of austenite during annealing increased strength in both base metal and cross-weld tension tests in the higher copper alloys. Furthermore, the stress associated with the onset of solidification cracking increased with increasing strength in the higher copper alloys rather than with increasing values of the Kou crack susceptibility index in the higher copper alloys. This work shows that higher copper content than typically allowed in steel product specifications can be accommodated before significant mechanical property or weldability concerns arise.

Keywords

- Low-Carbon Dual-Phase Sheet Steel
- Weldability
- Residual Copper

Introduction

Electric arc furnace steelmaking utilizing a large amount of scrap generates approximately one-third of the greenhouse gas emissions that steelmaking from ore generates, with recycling rates of up to 90% (Ref. 1). However, as household and transportation electrification increase, the concentration of undesirable residual elements, most notably copper, in the scrap cycle is growing exponentially (Ref. 2). Excess copper content is known to cause surface cracking in steels during thermomechanical processing in the form of liquid metal embrittlement, known as "hot-shortness." Due to the difficulty of being removed during the steelmaking process, the most-common method of mitigating copper accumulation is pig iron (from ore) dilution. With the amount of residual copper in the scrap cycle projected to increase along with the demand for pig iron, mitigation efforts will only become more important (Ref. 3). Beyond hot-shortness, however, the effects of residual copper on downstream manufacturing processes, such as weldability and weld performance, have also not been explored.

In steels, copper is known to act as an austenite stabilizer, lowering the ferrite-austenite transformation temperature and increasing the austenitic phase fraction at a given intercritical temperature. This increase in thermodynamic stability of austenite subsequently affects microstructure evolution during intercritical annealing, potentially yielding a higher fraction of the non-ferritic, or martensitic/austenitic (MA) constituents in dual-phase automotive sheet steels. The relative amounts and compositions of these microstructural constituents drastically affect the mechanical properties

<https://doi.org/10.29391/2025.104.025>

Table 1 – Compositions and Carbon Equivalent for All Base Materials (wt-%)

Alloy	C	Mn	Si	Cr	Cu	CE
0Cu	0.1	1.81	0.17	0.46	0.02	0.49
28Cu	0.1	1.99	0.24	0.5	0.28	0.55
83Cu	0.1	1.97	0.25	0.48	0.83	0.58
83Cu_RMn	0.1	1.76	0.25	0.49	0.83	0.55

of the base metals that must be welded during auto body fabrication (Ref. 4). In addition to austenite phase stability, copper is also known to increase steel hardenability. While several metrics may be used to quantify hardenability, the most common are critical diameter for bulk heat treatment processes and carbon equivalent in welding (Ref. 5).

Laser welding is a widely used industrial joining application due to its precision and speed (Ref. 6). This weld process is often used to join sheet steel sections during continuous annealing and automotive fabrication. The microstructure that develops in the heat-affected zone (HAZ) is particularly important regarding a weld's mechanical performance, as this is a common failure initiation site during service (Refs. 7–9). Due to the influence of copper on phase stability and hardenability, increased copper content will likely influence microstructure evolution in the HAZ and, therefore, weld performance.

This work aims to assess the influence of residual copper content on the laser weldability and weld performance of an automotive sheet steel. The influence of copper content on mechanical properties was evaluated using tensile tests of both the base metal and autogenously laser-welded joints and hardness profiles around the welds. The Sigmajig test, utilizing autogenous laser welding, was used to assess the influence of copper on solidification cracking susceptibility. A method to account for the influence of accumulating copper by decreasing manganese content was explored, guided by carbon equivalent calculations. The results of this work are expected to shed light on the future of fabrication with increased copper contents in steel products.

Experimental Procedures

Base Metal Composition, Design, and Production

A typical composition of a low-carbon dual-phase automotive sheet steel was used for this study with increasing amounts of residual copper up to 0.83 wt-%, which exceeded amounts normally seen in production (Refs. 10, 11), as shown in Table 1. The first three alloys had nominally the same base alloy composition with increasing copper content. Table 1 shows the carbon equivalent for each alloy, calculated using Equation 1 (Ref. 12).

$$CE = C + \frac{Mn}{6} + \frac{Cu + Ni}{15} + \frac{Cr + Mo + V}{5} \quad (1)$$

where CE is the carbon equivalent, and C , Mn , Cu , Ni , Cr , Mo , and V are the respective compositions in wt-%. It can be seen from Equation 1 and Table 1 that increasing copper content leads to a higher carbon equivalent and, thus, increased hardenability. The fourth composition contained the highest copper content evaluated in this study (0.83 wt-%) but with reduced manganese content to decrease the carbon equivalent to that of the alloy containing 0.28 wt-%. The purpose of the reduced manganese was to evaluate whether a reduction in other alloying elements, guided by a simple metric such as carbon equivalent, can be utilized to counteract the hardenability imparted by increased residual copper content.

All compositions were laboratory melted and cast by Cleveland-Cliffs, hot rolled to 16 mm thick, then cold rolled to a final thickness of 1.5 mm. Alloys were then intercritically annealed at 750°C for 5 h prior to forced air cooling to room temperature. The selection of the intercritical annealing temperature is described in subsequent sections.

Thermodynamic Simulations

To select the appropriate heat treatment temperatures, single-axis equilibrium simulations of phase fraction versus temperature were performed in Thermo-Calc 2024a software using the TCFE13 database. Specifically, the amount of austenite and ferrite were simulated between 600–850°C. The results of these simulations, which guided the heat treatment temperature, are described in the results section.

Gulliver-Scheil solidification simulations were also performed to determine the Kou crack susceptibility index (CSI) for each composition using Equation 2 (Ref. 13),

$$\left| \frac{dT}{d(f_s^{1/2})} \right| \left| \frac{dT}{d(f_s^{1/2})} \right|_{as} (f_s)^{1/2} \rightarrow 1 \quad (2)$$

where $\left| \frac{dT}{d(f_s^{1/2})} \right|$ is the slope of the temperature vs. the

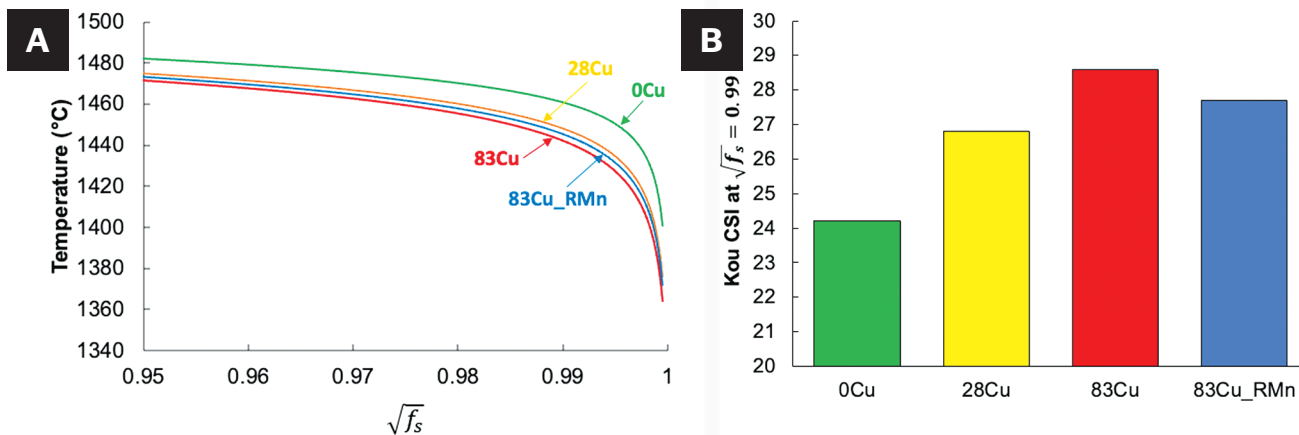


Fig. 1 – A – Gulliver-Scheil simulations; B – Kou CSI values for each alloy.

Table 2 – Equilibrium Amount of Austenite (γ) Predicted at 750°C

Alloy	0Cu	28Cu	83Cu	83Cu_RMn
Vol-% γ	36	45	53	48

square root of solid fraction curve taken between (f_s) of 0.85 and 0.99. Predictions of crack susceptibility were compared against weldability results aimed at determining the susceptibility to solidification cracking.

Laser Welding Parameters

A 4 kW ytterbium fiber laser (YLS-4000) with an IPG D30 series welding head on a three-axis gantry was used for welding. Full penetration autogenous laser welds were performed using a power of 900 W and a travel speed of 30 mm/s with a 6 mm defocus. Argon was flowed at a rate of 12 ft³/h for shielding. Laser welds were performed transverse to the sheet rolling direction for all samples, including cross-tension and Sigma-jig hot cracking specimens, as described in the next section.

Weldability Testing

The Sigma-jig test, which applies tensile stress perpendicular to the welding travel direction (Ref. 14), was used to evaluate solidification cracking susceptibility. Samples for this test were machined to a 25 mm X 50 mm geometry and loaded to stresses of 234, 257, 280, 304, and 327 MPa (in the rolling direction) prior to autogenous laser welding. After testing, crack lengths were measured using light optical microscopy, and a % cracking metric was calculated by dividing the maximum crack length by the length of the weld.

Hardness and Tensile Testing

Samples were sectioned perpendicular to the weld travel direction for hardness measurements using a LECO AMH55 automated microhardness indenter. Indents were made using

a 100 g load in three rows spaced 400 μ m along the thickness of the sheet, each with 60 indents spaced 100 μ m apart to span the width of the weld. This grid of indents captured hardness variations across the fusion zone, HAZ, and base metal.

Tensile tests were performed using an MTS Alliance RT/100 electromechanical load frame with an engineering strain rate of 10⁻⁴ s⁻¹ at room temperature and a Shepic extensometer with a 25 mm gauge length. Subsize ASTM E8 tensile test specimens with a 6 mm gauge width, 1.5 mm thickness, and 32 mm parallel length were used for the base metal and cross-welded samples. In cross-welded samples, the autogenous laser weld was placed in the center of the parallel length.

Microscopy

Samples were metallographically polished and etched with 1% nitric acid in ethanol prior to imaging using a Tescan S8252G SEM, with a 20 keV accelerating voltage and 10 nA beam current, using a secondary electron detector. The same SEM imaging settings were used to evaluate fracture surfaces from Sigma-jig testing. Optical microscopy and macro photos of specimens were used for crack length measurements.

Results

Thermodynamic Simulations and Heat Treatment Temperature Selection

The amount of austenite as a function of temperature was simulated for the alloys used in this study. Copper serves to stabilize austenite, so at a given temperature, there is predicted to be a higher phase fraction of austenite with increasing copper content. An annealing temperature of

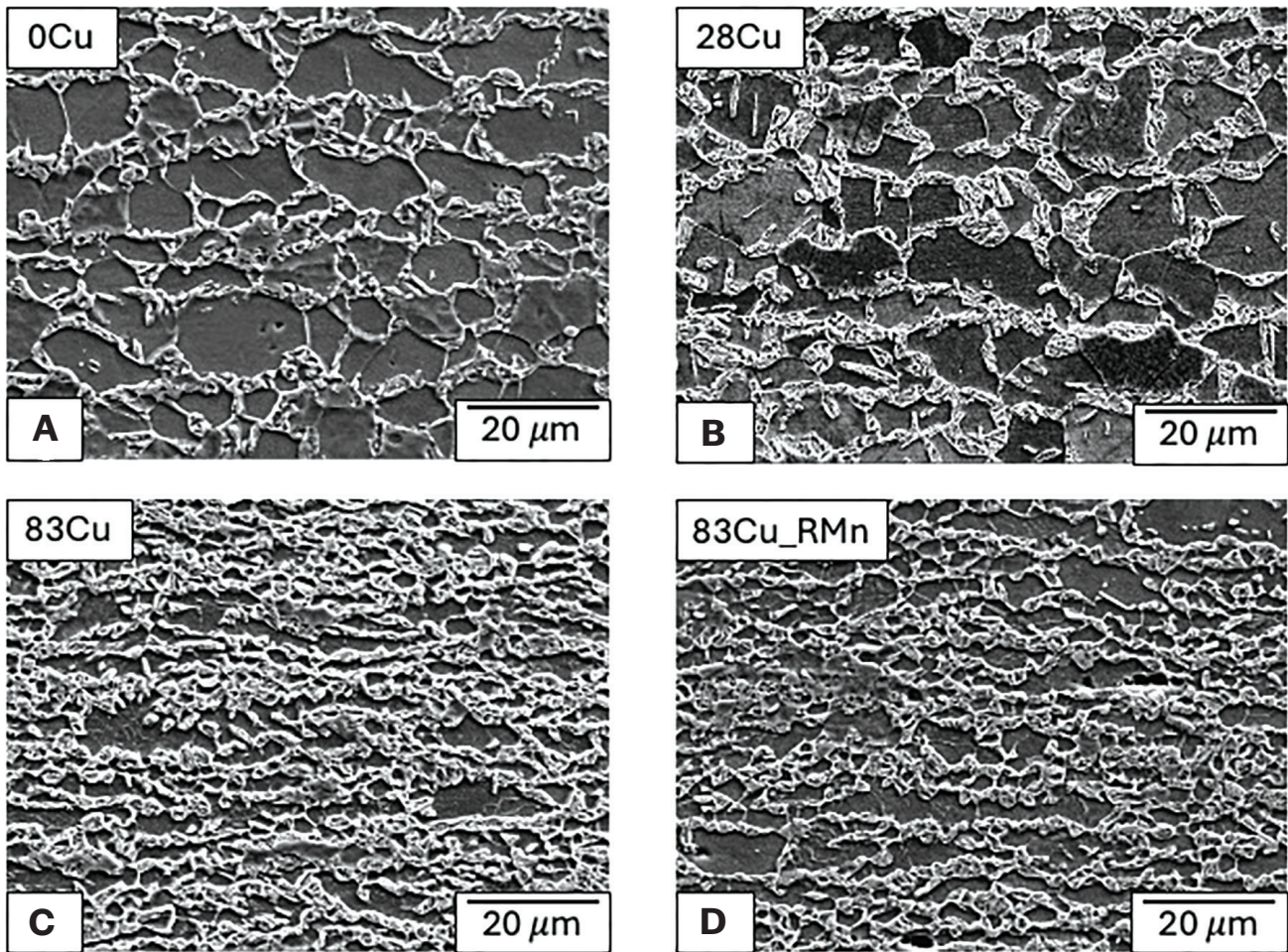


Fig. 2 – SEM micrographs of the intercritically annealed base metal for the following: A – 0Cu; B – 28Cu; C – 83Cu; D – 83Cu_RMn. All microstructures were etched with 1% nital.

750°C was selected to result in a range of austenite contents from 36–54% in all of the alloys, as shown in Table 2. Initial experimentation found that lower annealing temperatures (~700°C or below) were found to require very long times (> 10 h) to produce ferrite recrystallization, while higher temperatures (~800°C or higher) resulted in complete austenitization of the higher copper content alloys. It can be seen that the reduction of manganese in the 83Cu_RMn alloy reduced the amount of austenite stable at 750°C to nearly the same as the 28Cu alloy that had the same carbon equivalent.

The results of Gulliver-Scheil simulations used to calculate the Kou CSI are shown in Fig. 1A. Figure 1B shows that the CSI values generally increased with increasing copper content, and the reduction in manganese content reduced the CSI nearly to the value of the 28Cu alloy with similar carbon equivalent.

Base Metal Microstructure and Tensile Properties

Micrographs of the base metal microstructures following intercritical annealing are shown in Fig. 2. All of the alloys showed a combination of ferrite (darker recessed features)

with a non-ferritic constituent that was likely a combination of martensite and retained austenite (brighter proud features), referred to as MA. The MA constituent was a remnant from the austenite formed during intercritical annealing. A higher fraction of MA constituent was present with increasing copper content, concomitant with increases in the amount of austenite predicted to be present at 750°C, as summarized in Table 2. Additionally, the size of the ferrite grains decreased with increasing copper content. The reduction of manganese in the 83Cu_RMn alloy (Fig. 2D) did appear to have reduced the amount of MA relative to the 83Cu alloy (Fig. 2C) but not nearly to the degree of the 28Cu alloy, as thermodynamic simulations suggested. The ferrite grain size of 83Cu_RMn also appeared to be finer than that of 28Cu. In short, although reducing the manganese content may have led to a reduction in hardenability vis-à-vis reduced carbon equivalent, the base metal microstructure of 83Cu_RMn was more comparable to the 83Cu alloy than the 28Cu alloy.

Engineering stress-strain curves for each base metal are shown in Fig. 3. The addition of copper steadily increased yield strength and ultimate tensile strength while decreasing total elongation. Refinement in the microstructural scale, combined with more MA constituents due to copper,

as shown in Fig. 2, correlated with increased strength and reduced ductility observed. The reduction of manganese in the 83Cu_RMn alloy reduced the strength such that the yield and ultimate tensile strength were similar to the 28Cu alloy with similar carbon equivalent, but the ductility was only slightly improved compared to 83Cu. As might be expected from the microstructures in Fig. 2, the reduction in manganese did not fully compensate for increased copper content.

Laser Weld Microstructure, Hardness, and Tensile Properties

Figure 4 shows a hardness profile superimposed on a corresponding optical micrograph of an etched laser weld, using the 83Cu alloy as an example. It can be seen that the fusion zone (FZ) and the majority of the HAZ displayed higher hardness than the base metal. For all alloys, the HAZ region closest to the FZ exhibited the highest hardness, while the edge of the heat-affected zone nearest the base metal showed the lowest hardness. These regions are assumed to be the coarse-grained HAZ (CGHAZ) and subcritical HAZ (SCHAZ), respectively.

Laser weld hardness profiles for all alloys are compared in Fig. 5. The trends in base metal hardness reflected those seen in strength properties from tensile testing shown in Fig. 3, where higher hardness values were observed with increasing copper content. Similarly, the trends in the lowest hardness region of the heat-affected zone matched that of tensile properties (i.e., increasing copper content leads to higher hardness values), while the reduction of manganese reduced hardness in proportion to carbon equivalent. However, hardness trends in the FZ and CGHAZ were slightly different. The FZ and CGHAZ of the 83Cu and 28Cu alloys showed higher hardness than both 0Cu and 83Cu_RMn.

To provide some insight into the variation in hardness observed in Fig. 5, representative microstructures of the (A) lowest hardness region of the HAZ, (B) highest hardness region of the HAZ, and (C) center of the fusion zone are shown. The lowest hardness region of the HAZ very closely resembled that of the base metal, which explains why the trends in this region matched those of the base metal. Some degree of martensite tempering in the MA constituent was likely responsible for the

hardness reduction observed, as no other significant microstructural change was evident. However, the microstructures in the highest hardness regions of the HAZ and FZ appeared largely martensitic. The length of the martensite plates in the FZ appeared to be larger than those in the HAZ, indicating a larger prior austenite grain size compared to the CGHAZ. The finer martensite in the CGHAZ could explain the higher hardness relative to the FZ. Furthermore, the influences of copper content on austenite stability and resulting microstructure after intercritical annealing were no longer present in the FZ and high hardness region of the HAZ, so it stands to reason that the trends in hardness for these regions would be somewhat different compared to the base metal. It appears that the decrease in manganese lowered the hardness in martensitic regions to values comparable to those of the 0Cu alloy.

Engineering stress-strain curves for the cross-weld tensile samples are shown in Fig. 6A. The effects of copper and manganese content on cross-weld tensile properties closely resembled those observed in the base metal, as seen in Fig. 3, albeit at lower elongation ranges. Increasing copper content led to higher strength and lower ductility, while reducing manganese (in the 83Cu_RMn alloy) lowered strength comparable to the 28Cu alloy of the similar carbon equivalent.

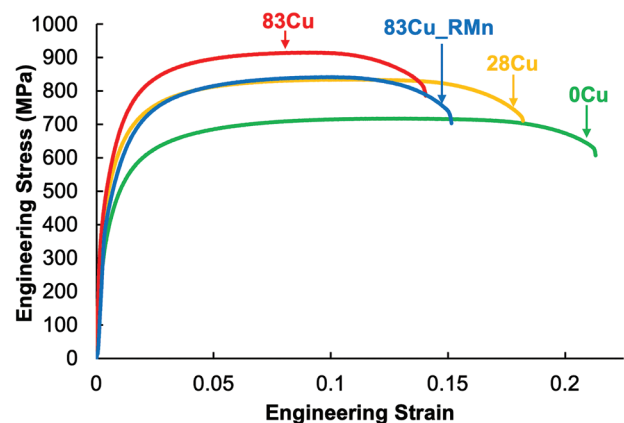


Fig. 3 — Engineering stress-strain curves for each base metal.

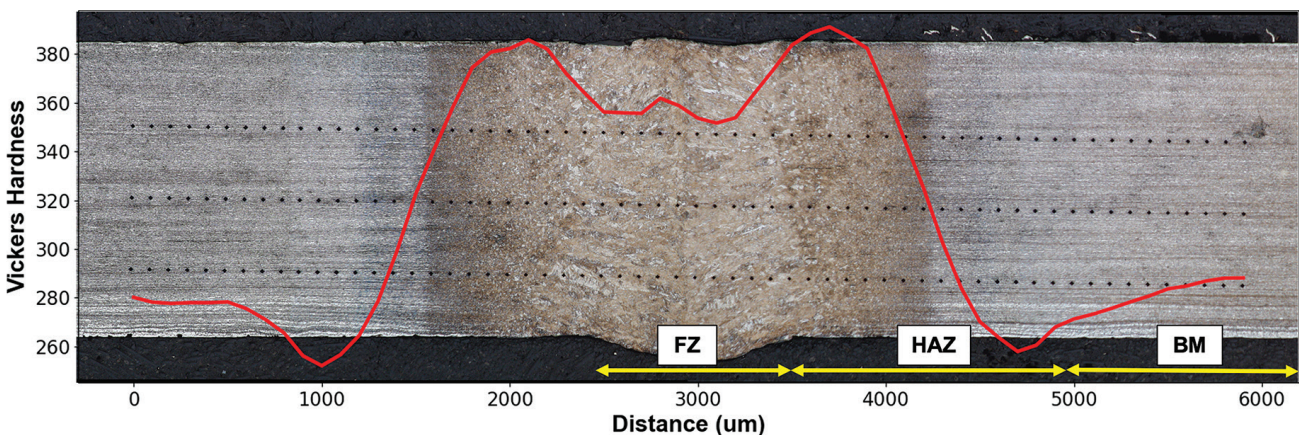


Fig. 4 — Vickers hardness vs. distance superimposed on an etched optical micrograph of a weld on the 83Cu alloy. The fusion zone, heat-affected zone, and base metal are highlighted.

Ductility in the 83Cu_RMn alloy was not recovered to the same degree compared to 28Cu, however. The ultimate tensile strengths of the cross-weld samples were similar to those of the base metal counterparts, but total elongation values decreased by nearly half. All samples necked near the softened region of the HAZ and failed in a ductile fashion

similar to the base metal, as shown in Fig. 6B. Considering that the majority of the weld fusion zone and heat affected zone showed higher hardness than the base metal, it would be expected that tensile behavior of the cross-weld samples would be controlled by properties of the base metal.

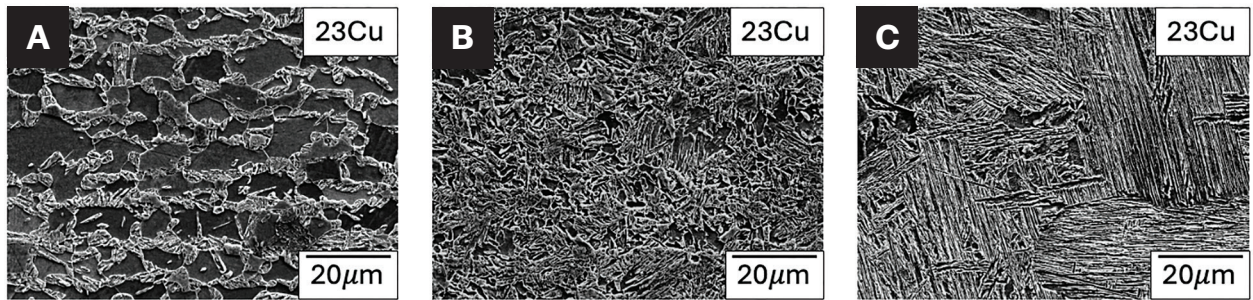
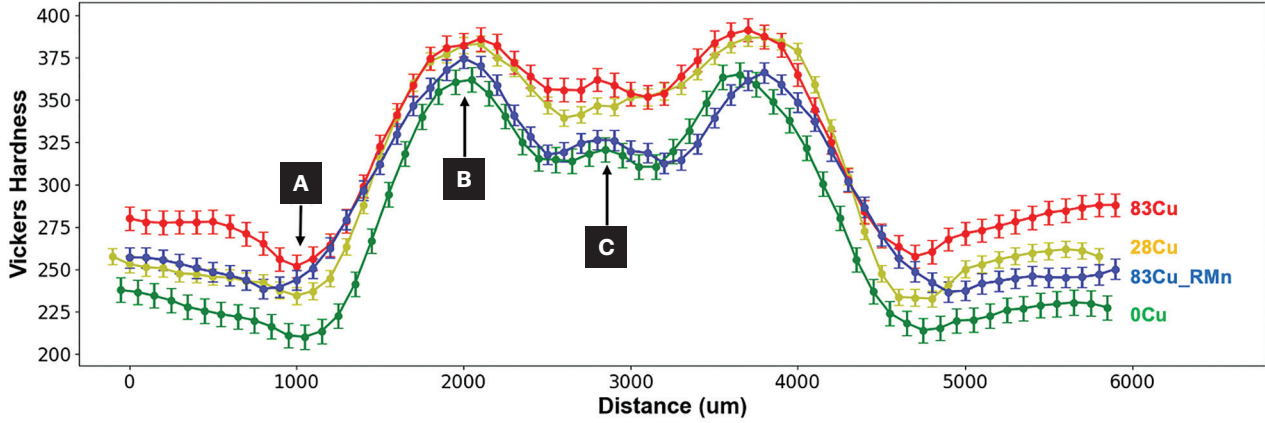


Fig. 5 – Hardness profiles of laser welds on all alloys. SEM SE micrographs of (top): A – Lowest hardness region of the HAZ; B – highest hardness region of the HAZ; C – center of the fusion zone. Error bars in the plot indicate 95% confidence intervals of the mean values at each location based on three hardness measurements.

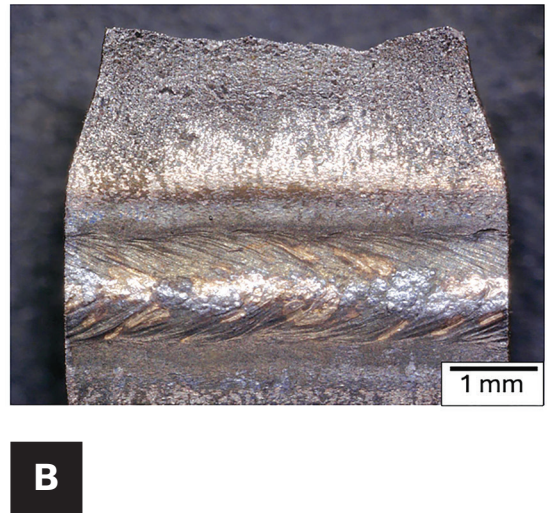
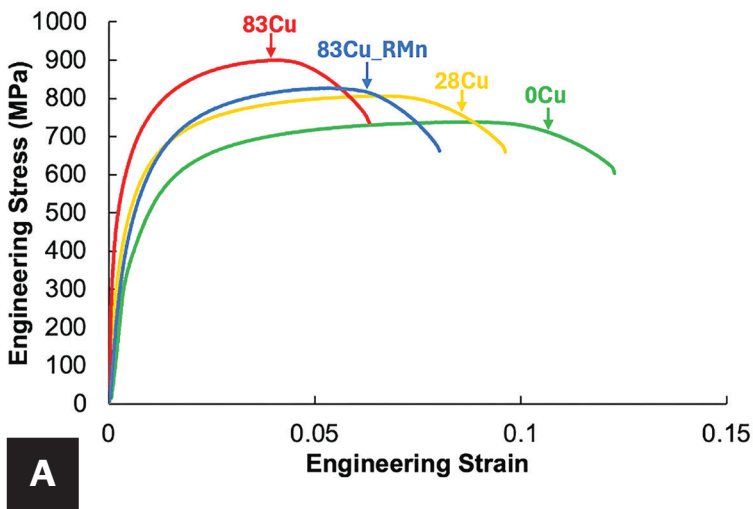


Fig. 6 – A – Engineering stress-strain curves of cross-welded samples of each alloy; B – representative macro photo of the neck and failure location of a cross-weld specimen

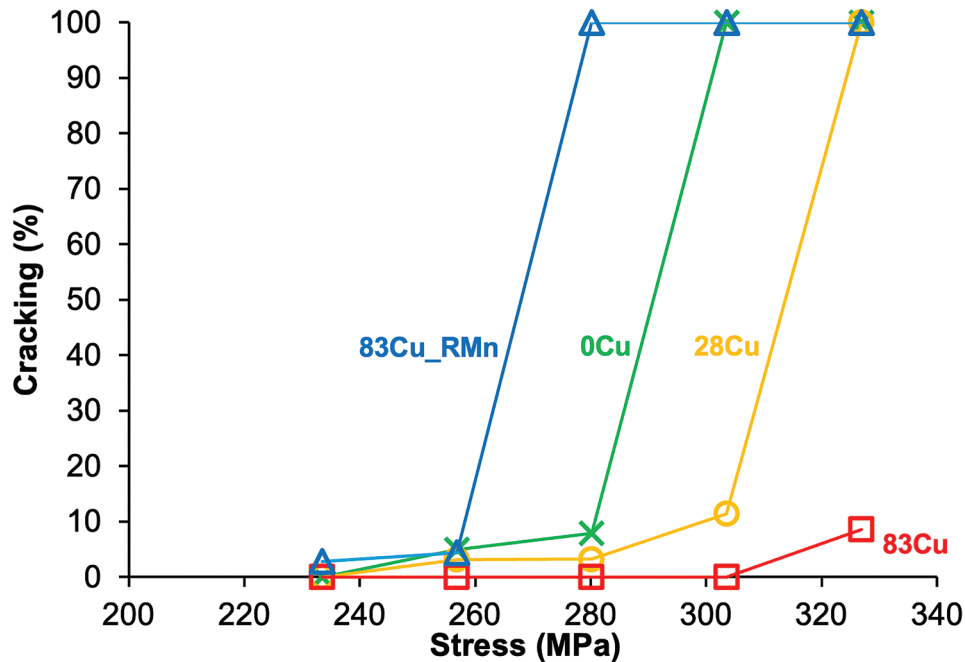


Fig. 7 – Sigmajig results of cracking % as a function of applied stress for the alloys with varying copper content.

Sigmajig Weldability Testing

The results of the Sigmajig testing are shown in Fig. 7 as cracking % vs. applied stress. With increasing stress, each alloy showed a rather abrupt transition from negligible to complete (100%) cracking, indicative of high solidification cracking resistance (Ref. 14). Sufficiently high stress could not be achieved to result in 100% cracking for the 83Cu alloy, but the onset of cracking was achieved at the highest stress used in this study. The stresses associated with the onset of cracking increased with copper content, which was opposite to the trends in CSI shown in Fig. 1. The decrease in manganese for the 83Cu_RMn alloy resulted in the lowest stress for the onset of cracking compared to all other alloys, disproportionately lower than the 28Cu alloy with similar CE and CSI.

All of the conditions that showed any degree of cracking, less than complete separation, exhibited a 30–50% decrease in stress after the test, indicating plastic deformation during welding. To determine whether extensive plastic deformation occurred, the fracture surfaces of a sample that exhibited complete separation were evaluated. Figure 8 shows macro images and fractographs of a sample that exhibited complete separation after testing. The majority of the weld (left side of Figs. 8A and B) was highly deformed, displaying a significant reduction in area with microvoid coalescence along the surface (Figs. 8C and D). Only the very end of the weld (right side of Figs. 8A and B) exhibited brittle, flat fracture with no discernible reduction in area and a fracture surface perpendicular to the applied stress. This region displayed what appeared to be dendrites on the fracture surface, indicating that solidification cracking likely occurred. It is likely that the majority of the weld yielded and ruptured in a ductile manner, while solidification cracking was limited to only the end of the weld.

In the samples that showed some degree of cracking, but not complete separation, thinning of the weld (but not complete ductile fracture) was observed with what appeared to be solidification cracking at the end of the weld, as shown in Fig. 9. Overall, it appears that the trends observed in weldability testing were primarily influenced by variations in the strength of the material instead of variations in predicted solidification cracking susceptibility, which indicates all of the alloys were quite resistant to solidification cracking and weldable.

Discussion

Base Metal Microstructure and Hardenability

As shown in Fig. 2, the relative amounts of ferrite vs. MA constituents in the base metal varied as a function of copper content. At a given intercritical annealing temperature, higher copper content increased the thermodynamic stability of austenite, while the reduction of manganese content lowered austenite stability, as summarized in Table 2. Upon cooling, whatever amount of austenite that formed during intercritical annealing likely transformed into some amount of martensite (and/or potentially bainite, although this was not evaluated here), with the amount of austenite formed during annealing having a direct impact on the amount of MA in the final microstructure. This trend was also reflected in the hardness of the base metal, which steadily increased with copper content (and lowered with reduced manganese content). Further, the base metal microstructures showed that the average ferrite grain sizes decreased as copper content increased, likely due to the increased amount of formed austenite that effectively subdivided the ferrite grains. Solute copper may also act to

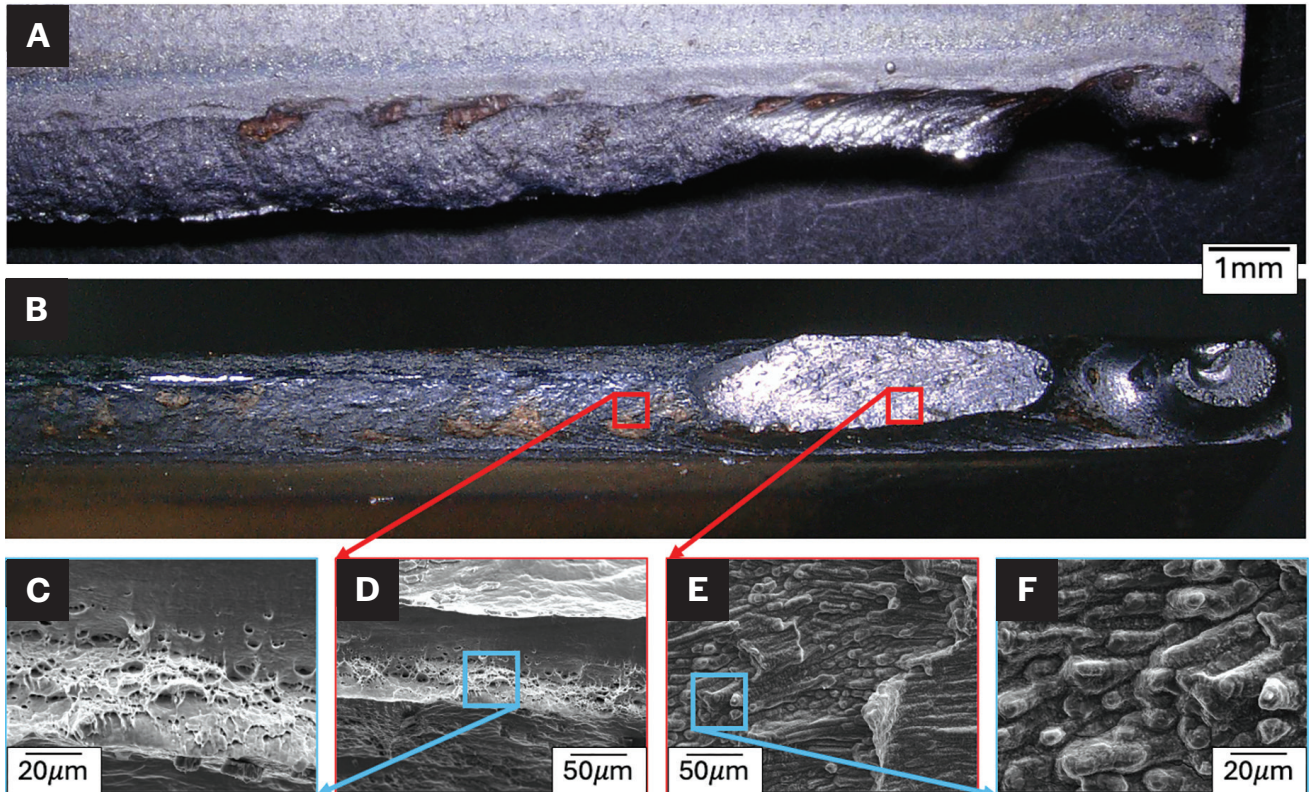


Fig. 8 – A representative sample from the 0Cu alloy showed 100% cracking at 303 MPa. Light optical macrographs oriented include: A – Down on the sample; B – toward the fracture surface. SEM SE micrographs of C and D – fracture surface along necked region; E and F – fracture surface exhibiting flat fracture perpendicular to the applied stress.

impede grain boundary motion through solute drag, further contributing to microstructural refinement (Refs. 15–17).

Carbon equivalent (CE) is essentially an indicator of hardenability and, more specifically for welding, the capacity of a steel to form martensite upon rapid cooling after welding (Ref. 5). Relative to manganese, copper has a relatively small but still positive contribution to hardenability, as shown in Equation 1. The reduced manganese alloy, 83Cu_RMn, was designed with this in mind (to achieve a CE comparable to alloy 28Cu) (Ref. 18). All heats displayed a similar hardness profile shape, as shown in Figs. 4 and 5. In particular, all exhibited a slight softening in the SCHAZ, a peak in hardness at the CGHAZ, and some intermediate hardness in the FZ. Despite differences in CE as a function of copper content, negligible differences in the size of the HAZ were observed. This could have been due to the highly localized nature of the HAZ following large temperature gradients during the weld.

Hardness in the Heat-Affected Zone

Softening of the SCHAZ was evident for all alloys tested, but it was most prominent in the 28Cu and 83Cu heats. This softening was likely due to tempering of the martensite in the MA constituent from the base metal. It has been observed elsewhere that alloys with higher fractions of martensite exhibit a higher degree of softening in the SCHAZ (Ref. 9). However, it should be noted that the reduction of manga-

nese in the 83Cu_RMn heat lowered the degree of softening. Hardnesses in the CGHAZ and FZ were shown to increase with the addition of copper and decrease with the reduction in manganese content. Unlike the base metal or SCHAZ, trends in hardness in the FZ and CGHAZ were not influenced by the microstructural constituents from the base metal. Because these regions were largely martensitic, differences in hardness were likely attributable to composition and associated solid solution strengthening. Copper imparts strengthening on the order of 52 MPa/wt-%, and manganese is similar at 44 MPa/wt-% (Ref. 19). For the compositional range explored here, an increase in solid solution strengthening of approximately 42 MPa could have been expected from increasing copper content alone. Using a proportionality constant of 2.876 (between changes in yield strength and hardness) (Ref. 20), this would have translated to a hardness increase of approximately ~15 HV due to copper content. The observed increases in hardness from the lowest to highest copper content ranged from 10–30 HV in Fig. 5, which may have also included unaccounted changes in carbon, nitrogen, and silicon content and associated solid solution strengthening.

Base Metal and Cross-Weld Tensile Properties

The engineering stress-strain curves for each base material shown in Fig. 3 all exhibited continuous yielding and

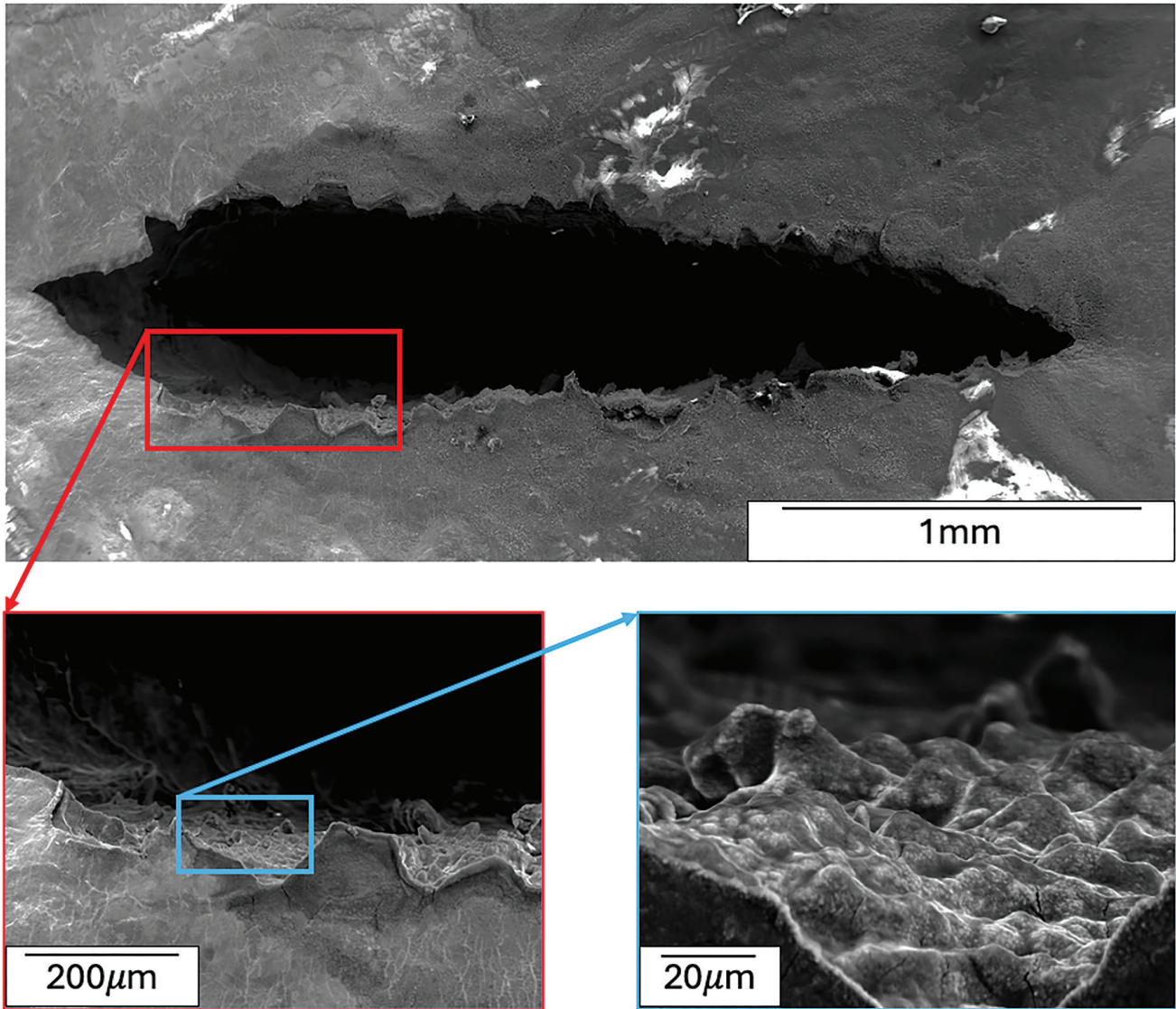


Fig. 9 – SEM SE micrograph of a partial crack interior (28Cu at 304 MPa), showing what appears to be dendrites on the fracture surface.

relatively high strain-hardening, typical for intercritically annealed dual-phase steels. The addition of copper steadily increased tensile strength while decreasing elongation to failure. For the high copper alloys, a decrease in manganese content was shown to lower tensile strength to that of the 28Cu heat while only partially recovering some ductility. The dominant contributor to these variations in tensile behavior was likely differences in the amount of the MA constituent. However, solid solution strengthening due to increased substitutional copper also played a relatively smaller role, with a predicted contribution of approximately 42 MPa for the highest copper composition explored in this work.

The cross-weld tensile tests outlined in Fig. 6 followed similar trends to the base metal (i.e., copper imparting higher strength and lower ductility). Compared to their base material counterparts, tensile strengths of the cross-welded samples were similar; however, elongation to failure decreased by approximately 30–40% for all alloys. Failure occurred near

the lowest hardness region of the HAZ for all materials, which is likely why the tensile behavior so closely resembled that of the base metal. The reduction in ductility in the cross-welded samples may have resulted from the high hardness weld and HAZ acting to restrain lateral contraction during tensile deformation, introducing some degree of triaxiality to the stress state.

Weldability

Gulliver-Scheil simulations in ThermoCalc predicted a steady increase in the solidification cracking susceptibility via the Kou CSI with the addition of copper and a slight decrease with reduced manganese. It should be noted, however, that the range in CSI values for the alloys evaluated here (20–30°C) was quite low compared to other alloy systems, such as Al-Cu (200–1600°C) reported by Kou (Ref. 13). The low CSI values implied that the alloys evaluated here should

be quite resistant to solidification cracking, which was certainly reflected in the Sigmajig results. The Sigmajig results in Fig. 7 displayed rather abrupt increases in cracking with increasing applied stress. That is, a sample either barely cracked or failed completely, with only a slight increase in stress. This abrupt behavior occurred when extensive plastic deformation occurred during welding, and when the elevated temperature ultimate tensile strength was reached, the sample failed in a ductile manner. A more moderate increase in the amount of cracking with higher applied stresses is typically observed for alloys susceptible to solidification cracking (Ref. 14). Further, no alloy at any stress level evaluated showed complete fracture by solidification cracking. Partially cracked samples exhibited solidification cracking at the end of the weld, with the remaining portion of the weld considerably thinned due to plastic deformation. Full width failures also showed a small amount of solidification cracking at the end of the weld with extensive reduction in thickness and ductile fracture throughout the remaining majority of the weld length, as seen in Fig. 8. Considering the extensive plastic deformation in all conditions displaying any cracking at all, the Sigmajig results reflected the effect of copper on strength in what was essentially a hot tensile test, as opposed to solidification cracking susceptibility per se. However, the reduction in manganese in the 83Cu_RMn alloy appeared to have reduced the stress threshold for the onset of cracking to a much greater degree than would be expected from its strength relative to the other alloys. The negative influence of reduced manganese on the onset of cracking, in excess of what would be expected from the observed decrease in strength, requires more investigation.

Outlook for Increased Residual Copper in Welded Sheet Steels

Overall, the effects of increased residual copper on laser weldability of dual-phase steels were found to be highly dependent on base metal microstructure. Under fixed intercritical annealing conditions, microstructures of the alloys with increased copper content showed finer ferrite grain sizes and more MA constituents, which heavily influenced nearly all downstream mechanical properties, welded or otherwise. If the intercritical annealing treatments had been tailored for each composition to achieve more comparable microstructures, differences in strength properties would have likely been minimized. This work evaluated the efficacy of using carbon equivalent to guide alloy design to compensate for the effects of increased copper content. Although reducing manganese content appears to have reduced strength properties, ductility was not fully recovered. Furthermore, reductions in manganese reduced weldability to a greater degree than would be expected from tensile properties. Overall, it appears that the dual-phase sheet steels evaluated here can accommodate increases in residual copper without drastic debits in weldability and weld performance, but careful consideration of the influences of copper on the annealed base metal microstructure development must be taken.

Conclusions

This work aimed to assess the effects of increasing residual copper content on microstructure, laser weldability, and weld performance of a low-carbon dual-phase sheet steel. Carbon equivalent was used to account for the increased hardenability effects by reducing the manganese content. Microhardness and cross-weld tensile tests of autogenously laser-welded sheet were conducted and compared to base metal tensile properties to evaluate weld performance. The Sigmajig tests were performed to evaluate hot cracking susceptibility. The main conclusions of this work are as follows:

1. After intercritical annealing at 750°C for 5 h, the higher copper alloys showed a greater amount of MA constituent and finer ferrite grain size due to a greater amount of austenite present during annealing. The increase in austenite at the intercritical annealing temperature was predicted with thermodynamic simulations.
2. Base metals with higher copper content exhibited increased yield and tensile strength but decreased ductility. While copper solid solution strengthening may have played a role, the differences in ferrite grain size and MA amounts likely contributed most to variations in tensile properties.
3. Autogenous laser welds of all alloys showed similar hardness profiles where the fusion zone and the majority of the heat-affected zone exhibited higher hardness than the base metal. The heat-affected zone closest to the base metal showed some softening, likely due to the tempering of martensite in the MA constituent.
4. The trends in cross-weld tensile behavior were the same as in the base metal. All cross-weld tensile samples necked at the lowest hardness region of the heat-affected zone and failed in a ductile fashion.
5. A reduction in manganese content, guided by calculations of carbon equivalent, was shown to reduce strength-related tensile properties of the base metal and cross-weld samples, but ductility was not fully recovered.
6. All of the materials were observed to exhibit extensive plastic deformation, while minor solidification cracking was observed in the Sigmajig tests. This led to an increase in stress for the onset of cracking with increasing copper content, concomitant with increases in base metal strength. The reduction in manganese was found to decrease the stress for the onset of cracking to a greater degree than base metal tensile properties would suggest.

Declaration of Competing Interest

The authors declare that they have no known competing financial interests or personal relationships that could have appeared to influence the work reported in this paper.

Acknowledgments

This work was supported by the Department of Energy's Advanced Manufacturing Office under Grant No. DE-EE0009389. Data analysis was supported by instrumentation acquired through the support of the National Science Foundation (DMR-1828454).

Author Contribution Statement

Henry Geerlings: Conceptualization, Methodology, Investigation, Formal Analysis, Writing – Original Draft, Writing – Review and Editing

Grant Thomas: Resources, Writing – Review and Editing

Amy Clarke: Funding Acquisition, Writing – Review and Editing

Kester Clarke: Funding Acquisition, Project Administration, Writing – Review and Editing

Jonah Klemm-Toole: Funding Acquisition, Conceptualization, Methodology, Supervision, Writing – Review and Editing

References

1. Daehn, K. E., Cabrera Serrenho, A., and Allwood, J. M. 2017. How will copper contamination constrain future global steel recycling? *Environmental Science and Technology* 51(11): 6599–6606. DOI: 10.1021/acs.est.7b00997

2. Daehn, K. E., Cabrera Serrenho, A., and Allwood, J. M. 2019. Finding the most efficient way to remove residual copper from scrap steel. *Metallurgical and Materials Transactions B* 50(3): 1125–1140. DOI: 10.1007/s11663-019-01537-9

3. Allwood, J. M., Cullen, J. M., and Milford, R. L. 2010. Options for achieving a 50% cut in industrial carbon emissions by 2050. *Environmental Science and Technology* 44(6): 1888–1894. DOI: 10.1021/es902909k

4. Rashid, M. 1981. Dual phase steels. *Annual Review of Materials Research* 11: 245–266.

5. Kasuya, T., and Hashiba, Y. 2007. Carbon equivalent to assess hardenability of steel and prediction of HAZ hardness distribution. *Nippon Steel Technical Report* 95.

6. Hong, K.-M., and Shin, Y. C. 2017. Prospects of laser welding technology in the automotive industry: A review. *Journal of Materials Processing Technology* 245: 46–69. DOI: 10.1016/j.jmatprotec.2017.02.008

7. Fairchild, D. 1990. Fracture Toughness Testing of Weld Heat-Affected Zones in Structural Steel. In *Fatigue and Fracture Testing of Weldments* STP1058-EB: O. DOI: 10.1520/STP24093S

8. Yilbas, B. S., Arif, A. F. M., and Abdul Aleem, B. J. 2010. Laser welding of low carbon steel and thermal stress analysis. *Optical and Laser Technology* 42(5): 760–768. DOI: 10.1016/j.optlastec.2009.11.024

9. Khan, M. S., Soleimani, M., Midawi, A. R. H., Aderibigbe, I., Zhou, Y. N., and Biro, E. 2023. A review on heat affected zone softening of dual-phase steels during laser welding. *Journal of Manufacturing Processes* 102: 663–684. DOI: 10.1016/j.jmapro.2023.07.059

10. Llewellyn, D. T., Marriott, J. B., Naylor, D. J., and Thewlis, G. 1980. The effects of residual elements on the properties of engineering steels. *Philosophical Transactions of the Royal Society A* 295(1413): 69–85. DOI: 10.1098/rsta.1980.0076

11. Sousa, M. N., Evangelista Luiz, N., De Oliveira, D. C., De Souza Barrozo, M. A., and Machado, Á. R. 2012. Effect of residual chemical elements (Cr, Ni and Cu) on machinability of leaded low carbon free machining steels. *Materials Science and Technology* 28(2): 220–226. DOI: 10.1179/1743284711Y.0000000022

12. Kasuya, T., and Yurioka, N. 1993. Carbon equivalent and multiplying factor for hardenability of steel. *Welding Journal*.

13. Kou, S. 2015. A criterion for cracking during solidification. *Acta Materialia* 88: 366–374. DOI: 10.1016/j.actamat.2015.01.034

14. Goodwin, G. M. 1987. Development of a new hot-cracking test – The Sigamjig. *Welding Journal* 66(2): 33–38.

15. Takaki, S. et al. 2004. Effect of copper on tensile properties and grain-refinement of steel and its relation to precipitation behavior. *Materials Transactions* 45(7): 2239–2244. DOI: 10.2320/matertrans.45.2239

16. Aaronson, H. I., Reynolds, W. T., and Purdy, G. R. 2004. Coupled-solute drag effects on ferrite formation in Fe-C-X systems. *Metallurgical and Materials Transactions A* 35(4): 1187–1210. DOI: 10.1007/s11661-004-0294-2

17. Rana, R., Bleck, W., Singh, S. B., and Mohanty, O. N. 2007. Laboratory investigations on copper-alloyed interstitial free steel – Part I: Effect of annealing. *Steel Research International* 78(8): 612–621. DOI: 10.1002/srin.200706257

18. Calcagnotto, M., Ponge, D., and Raabe, D. 2012. On the effect of manganese on grain size stability and hardenability in ultrafine-grained ferrite/martensite dual-phase steels. *Metallurgical and Materials Transactions A* 43(1): 37–46. DOI: 10.1007/s11661-011-0828-3

19. De Cooman, B. C., and Findley, K. 2017. Introduction to the mechanical behavior of steel. *Association for Iron & Steel Technology*.

20. Pavlina, E. J., and Van Tyne, C. J. 2008. Correlation of yield strength and tensile strength with hardness for steels. *Journal of Materials Engineering and Performance* 17(6): 888–893. DOI: 10.1007/s11665-008-9225-5

HENRY GEERLINGS, AMY CLARKE, KESTER CLARKE, and JONAH KLEMM-TOOLE (jklemmto@mines.edu) are with the George S. Ansell Department of Metallurgical and Materials Engineering, Colorado School of Mines, Golden, Colo. **GRANT THOMAS** is with Cleveland-Cliffs Inc., Research & Innovation Center, Middletown, Ohio.